Application of Shape Memory Alloy Torsion Tube in Folding Wingtip Mechanism of Morphing Aircraft

LAI Zhenyang, WANG Chen*, YANG Yang, WAN Liliang, SHEN Xing

College of Aerospace Engineering, Nanjing University of Aeronautics and Astronautics, Nanjing 210016, P. R. China

(Received 23 May 2025; revised 16 July 2025; accepted 11 August 2025)

Abstract: Morphing aircraft are designed to adaptively adjust their shape for changing flight missions, which enables them to improve their flight performance significantly for future applications. The folding wingtips represent a key research aspect for morphing aircraft, since they can lead to potential improvements in flight range, maneuverability, load alleviation and airport compatibility. This paper proposes a hinge mechanism design for folding wingtips based on the shape memory alloy torsion tube, aiming to achieve successful folding using the actuation effect of the shape memory alloy. The proposed design employs a shape memory alloy torsion tube as the actuator for the active folding of the wingtip, which is motivated by the characteristics of the tube, enabling a simplified structure for the integration with high energy density. Through numerical simulation and testing of the folding wingtip structure, the concept is verified, which shows its potential as an actuator for folding wingtips.

Key words: morphing aircraft; folding wingtip; shape memory alloy torsion tubes

CLC number: V224.3 **Document code:** A **Article ID:** 1005-1120(2025)S-0078-13

0 Introduction

The application of folding wingtip technology is a common feature of modern aircraft design, particularly in the case of naval and large transport aircraft^[1]. The folding wingtip can be retracted both on the ground and in flight, substantially reducing the parking space and enhancing airport compatibility. Furthermore, the active folding of the wingtip during flight can serve to reduce induced drag and optimize aerodynamic characteristics, thereby enhancing flight performance. For example, naval fighters use wingtip folding technology to reduce their footprint on the ship. The in-flight folding wingtip system, inspired by the XB-70 Valkyrie, offers considerable aerodynamic advantages, including augmented lift and directional stability. These attributes render it a promising solution for prospective applications in large civil aircraft^[2]. Wan et al.^[3] devised a hinged passive folding wingtip structure for the mitigation of gust loads in aircraft, and validated the efficacy of the folded wingtip load mitigation through flight testing. Mills et al. [4] examined the efficacy of folding wingtips as control effectors in enhancing the roll control of UAVs, demonstrating their considerable impact on the lateral and directional stability.

The efficacy of active folding wingtips is contingent upon the functionality of the actuator. The use of conventional mechanical actuators is often associated with a number of drawbacks, including complexity and weight, which may offset the performance gains offered by folding wingtips. To address these challenges, researchers have developed a range of efficient and lightweight actuators to enable precise control of the wingtip. Pan et al. [5] presented the current state of smart material actuators in the field of aerospace engineering. The ultrasonic motor based on the inverse piezoelectric effect was also used, with the aim of achieving remote, adaptive control of rudder deflection in wind tunnel tests. Fur-

^{*}Corresponding author, E-mail address: cwangaero@nuaa.edu.cn.

How to cite this article: LAI Zhenyang, WANG Chen, YANG Yang, et al. Application of shape memory alloy torsion tube in folding wingtip mechanism of morphing aircraft[J]. Transactions of Nanjing University of Aeronautics and Astronautics, 2025, 42(S):78-90.

thermore, the flexible folding wingtip structures, proposed by He et al.^[6], which was based on corrugated plates and honeycomb structures, demonstrated the potential for adaptive adjustment, enabling wingtip shape control with reduced weight.

The shape memory alloy (SMA) has been extensively employed in the aerospace, mechanical and bio-medical engineering^[7] because it has advantages in terms of energy density and structure integration. The application of SMA in folded wingtip actuators has increased gradually over recent years. It has been demonstrated that SMA actuators can effectively reduce weight of the system, and simplify the structural design and adapt well to the environment^[8]. Li et al.^[9] proposed an SMA spring-based actuator to control the wingtip folding angle by adjusting the temperature, which allowed the device to adaptively recognize the flight environment and adjust the folding angle accordingly. In the Smart Wing project^[10], SMA actuators were employed to deflect the control surface of the wing with improved performance. In the Spanwise Adaptive Wing project^[11], the utilization of SMA torsion tubes were used to change the dihedral angle of the outboard wing, which could be used for the flight control of aircraft.

SMA torsion tubes represent a compact actuation mechanism with high energy density, which has the potential for folding wingtip technology[12]. SMA torsion tubes exhibit a higher energy density and power-to-weight ratio than conventional drives, enabling them to provide a greater torque output and a wider range of torsion angles. In the context of the remote-control actuation[13] program, the SMA torque tube has been demonstrated to achieve an efficient torque output and maintain its performance under extreme conditions. Icardi et al.[14] demonstrated the feasibility of using SMA torsion tube actuators in an adaptive wing for a small UAV, highlighting their ability to provide sufficient power and torque while maintaining structural integrity for the wing shape control.

To sum up, the gain effect brought about by the implementation of wingtip folding technology in the vehicle is considerable since it can reduce the space occupied by the vehicle on the ground and adapt the environment, and improve aerodynamic performance and longitudinal maneuvering efficiency during flight. However, the design of the wingtip folding actuator has a considerable influence on its efficacy. The deployment of complex and heavy actuators could negate the advantages offered by wingtip folding. Consequently, the development of efficient and lightweight actuators represents a key aspect for future research. The potential of SMA torsion tubes as actuators has been demonstrated with sufficient energy density, power-to-weight ratio and stroke. But further work is required for the integration and application of the SMA tube actuator.

This paper presents the conceptual design of the folding structure from the wingtip in the first section. The second section outlines the actuator design based on the SMA torsion tube, which is necessary for the wingtip folding. Then, the folding capability and structural strength of the wingtip are analyzed, and the heating recovery ability of the SMA torsion tube is tested in a no-load condition, which can lay down the foundation for the future work.

1 Wingtip Folding Structure Design

The deployment of active wingtip folding technology represents a significant advancement in the field of modern aircraft design. This technology not only reduces the requisite parking space by diminishing the wingspan when the aircraft is on the ground, but also it enhances flight efficiency by curbing induced drag and optimizing aerodynamic performance during flight. Furthermore, wingtip folding technology enhances aircraft maneuverability, extends range and improves lateral stability in flight, rendering it an indispensable and innovative technology for future aircraft design. The design of an active wingtip folding mechanism within the limited space of a wingtip becomes a significant challenge. In order to design a wingtip folding structure suitable for ground testing, a conceptual model is presented in the current study, as illustrated in Fig.1. This model comprises the primary wing structure and the foldable wingtip component, and it employs

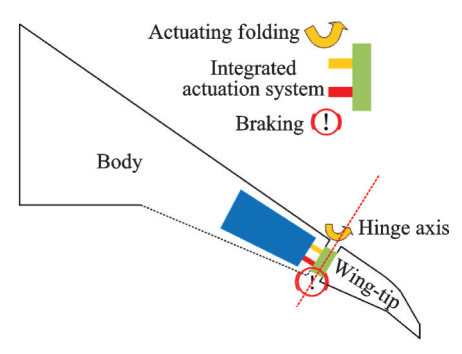


Fig.1 Conceptual model of an active folding wingtip

an integrated actuator system to facilitate control and braking of the wingtip folding mechanism.

The process of folding the wing tips of an aircraft primarily occurs in the following scenarios: When the aircraft is stationary at an airport or ship, the wingspan is reduced in order to minimize the aircraft's footprint; when the aircraft is in flight, the wingtips are not folded in order to reduce the induced drag, but can change the dihedral angle of the wingtip to work as a control surface of the wing. Nevertheless, the operational circumstances, is shown in Fig.2. The attitude of the vehicle during flight remains inherently unpredictable, with the wingtip subjected to a multitude of complex and variable loads. These encompass aerodynamic loads, inertial loads, structural loads, dynamic loads, and so on. It is essential that the design of the wingtip takes these loads into account. It is essential that the design of the wingtip considers the combined effects of these loads in order to guarantee the maintenance of structural strength, stiffness and stability under different flight conditions. Concurrently, the design of the folding mechanism must guarantee that it can safely and reliably complete the folding and unfolding tasks under these loads.

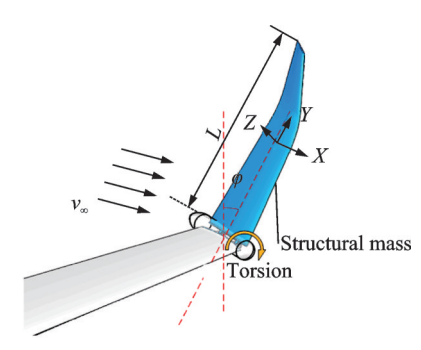


Fig.2 Conceptual model of folding wingtip loading

1. 1 Structural components of an active folding wingtip

The folding wingtip structure is illustrated in Fig.3. It comprises three principal components: The power element, the connecting structure, and the braking apparatus situated on the connecting structure and the gearing mechanism.

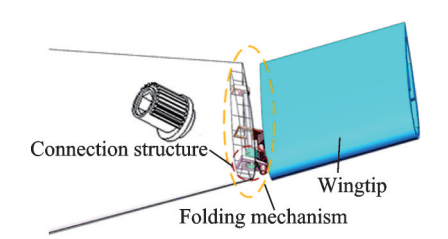


Fig.3 Wingtip folding structure

The objective of this study is to examine the actuation capability of the folding wingtip. Thus, the wing parameters have been simplified by employing the NACA2412 airfoil, with a foldable section chord length of 400 mm and a spread length of 400 mm. The output of the power element is connected to the connection structure depicted in Fig. 3. One of the gear sets is mounted in the connection structure, while the other is mounted on the gear shaft connected to the wing beam. The gear ratios are adjusted according to the torque of the power element and the angular output capability in order to achieve the desired folding effect of the wingtip at a specified angle. Furthermore, the connection structure at the output end is fixed by the standoffs, which simultaneously secure the bearings of the gear shafts at the wing beam.

As shown in Fig.4, in the connecting structure with the brake, the splined ends of the connecting head and torsion tube are arranged so that the rotation at one gear end can amplify the torsion-angle output. Concurrently, the braking apparatus depicted in Fig.4 is employed to regulate the rotation of the connecting structure. The locking mechanism comprises two upper and two lower friction discs, along with two sets of springs with different elasticity coefficients, which supports the two end caps. The two end caps are positioned on a support, with the upper part pre-tensioned using bolts. The upper

end cap is suspended on the connecting head, supported by the upper support spring. The lower support spring, with a higher elasticity coefficient, supports the two friction discs. The position of the pretensioning bolts is adjusted so that the two friction discs do not contact with the connecting head under non-braking conditions. It is necessary to adjust the position of the preloading bolt in order to prevent contact between the two friction discs and the connector under non-braking conditions. In the event of braking, the slot in which the electromagnet is mounted will be energized, enabling the two friction discs to overcome the spring support force and clamp the connecting structure, and achieve braking.

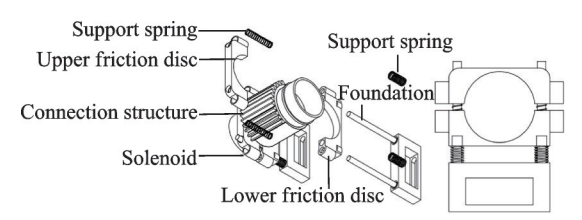


Fig.4 Braking device

1. 2 Transmission relationships for wingtip folding structures

In conjunction with the wingtip folding concept and structural design, the actuator load is input from the connecting structure, and the variable speed is realized by gearing. The applicable transmission relationship is selected according to the torque and cornering output effect of the actuator, considering the aforementioned factors. In regard to the folding structure, the load and displacement at the input are related to the wingtip folding angle and the load applied to it in the following manner.

$$i = \frac{n_2}{n_1} \tag{1}$$

where n_1 represents the number of gear teeth at the input end and n_2 the number of gear teeth at the output end. The gearing mechanism integrated into the wingtip structure has a direct impact on both the folding angle of the wingtips and the load characteristics of the drive mechanism. Furthermore, the relationship between the input angle of the driver and the folding angle of the wingtip can be expressed di-

rectly in accordance with the gear ratio.

$$\varphi_{\text{input}} = i\varphi_{\text{output}} \tag{2}$$

where φ_{input} is the angle of rotation of the input and φ_{output} the angle of rotation of the output. The required folding angle of the wingtip is determined according to the specific application scenario of the wingtip folding structure. This is achieved by selecting the appropriate gear parameters, which must consider the precision requirements of the wingtip folding as well as the angle of rotation input characteristics of the drive mechanism. In the process of wingtip folding, the load at the wingtip hinge is generated by the inertial force of the wingtip structure, the aerodynamic load, and the friction of the hinge. In a fixed coordinate system on the wingtip structure, the X-axis represents the chord length of the wingtip, the Y-axis indicates the direction of wingtip spreading, and the Z-axis denotes the vertical direction of the airfoil surface. The relationship between external loads and the input torque of the actuator can be expressed as follows

$$T_{\text{input}} = \frac{1}{i} \cdot \left(G_Z \cdot L_m + \int P_Z L_i \, dA + M A_Z L_m + T_f \right)$$
(3)

where $T_{\rm input}$ represents the torque at the input, G_Z the component of gravity of the wingtip structure along the Z-axis of the coordinate system, $L_{\rm m}$ the force arm, P_Z the component of aerodynamic loads on the wingtip surface along the Z-axis, L_i the force arm at the position of each micrometer area ${\rm d}A$, M the mass of the wingtip structure, A_Z the component of the wingtip structure acceleration along the Z-axis, and $T_{\rm f}$ the sum of the torque of the folding structure of the wingtip at its internal contact-generated friction as well as the other loads on the sum of torques at the output of the hinge structure.

2 Design and Analysis of the Actuator

SMAs are metal materials that undergo phase transformation in response to external stress and changes in environmental temperature, leading to deformation. This phase transformation enables SMAs to remember their initial shape. After com-

pleting the phase transformation within a certain range, the material will return to its original shape. By utilizing this deformation process, SMAs can be engineered into specific configurations for practical applications, achieving targeted actuation effects. Compared with other actuation materials, actuators based on SMAs offer simpler structures, higher energy density, and better power-to-weight ratios, making them particularly suitable for installation in the limited space of a wingtip.

By forming SMA into a tubular structure, precise shape control and torque output can be achieved through phase transformation. To ensure the feasibility of this effect in practical applications, the material properties of the torque tube must meet specific performance requirements, such as stable high torque output and precise control of the phase transformation temperature. Specifically, the phase transformation temperature of the torque tube in different environments directly determines whether it can effectively function. Therefore, accurately measuring the phase transformation temperature of the SMA torque tube is critical for ensuring controllability and reliability under operational conditions. Differential scanning calorimetry (DSC) is an effective method for accurately determining the phase transformation temperature of the torque tube under the intended usage environment.

The phase transformation temperature test results are shown in Fig.5. The martensitic transformation start temperature is $50.1~^{\circ}\mathrm{C}$, and the martensitic transformation finish temperature is $0.4~^{\circ}\mathrm{C}$. The austenitic transformation start temperature is $48~^{\circ}\mathrm{C}$, and the austenitic transformation finish temperature is $66.9~^{\circ}\mathrm{C}$. Based on the phase transformation temperature test results, the shear modulus of the material in both low-temperature and high-temperature states is measured, as shown in Fig.6. The shear modulus in the martensitic state is measured to be $12~\mathrm{GPa}$, while the shear modulus in the austenitic state is $20.5~\mathrm{GPa}$. The detailed parameters are shown in Table 1.

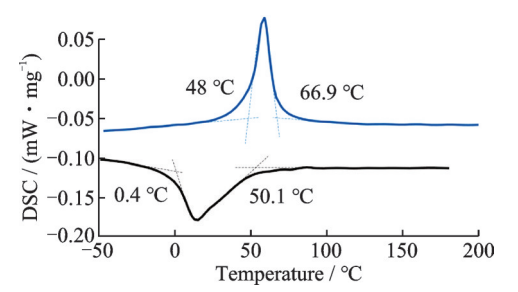


Fig.5 Transformation temperature test results

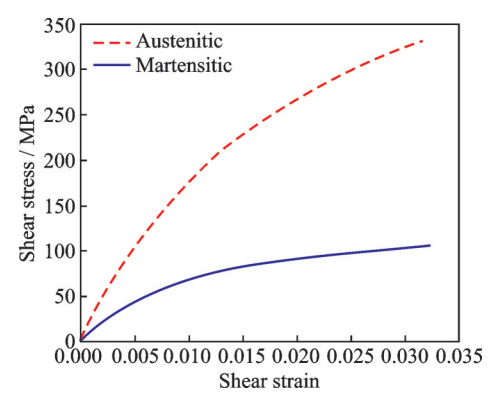


Fig.6 SMA torsion tube shear modulus

Table 1 SMA torque tube parameters

Parameter	Value
Inner diameter/mm	10
Outer diameter/mm	13
Actual length/mm	250
Effective length/mm	210
Output torque/(N•m)	32
Output angle/(°)	60
Shear strain/%	3.165

2. 1 Design of the bias mechanism

In this paper, the actuation effect is achieved through the utilization of the one-way shape memory effect of the SMA torsion tube. The matching bias mechanism exerts a significant influence on the torque and rotation angle output effect of the SMA torsion tube. As illustrated in Fig.7, the driving process and principle of the driving mechanism are as follows: The pre-twisted SMA torque tube is completed installed, and a part of the pre-stretching force is set to the bias tension spring. Starting heating, the SMA torque tube phase changes from the detwinned martensite to the austenite. This is illustrated by the change of the red arrow shown in Fig.7, which leads to the folding of the wingtip. Concurrently, the bias spring undergoes further

stretching, and a part of the energy is stored. As the temperature decreases, the material undergoes a gradual transformation to martensite. This results in a decrease in the shear modulus of the material, enabling the pre-stretched bias spring to induce the torsion process depicted by the blue arrows in Fig.7. This releases energy, causing the wingtips to fold downwards, while simultaneously transforming the torsion tube from twinned martensite to non-twinned martensite.

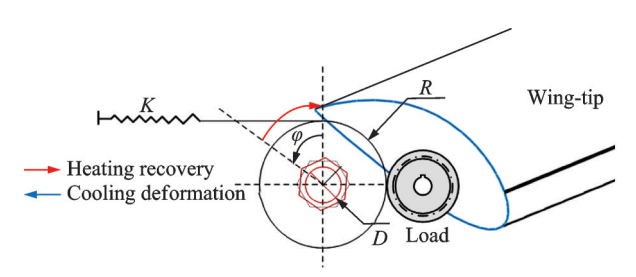


Fig.7 SMA torsion tube actuator principle

The mechanical test results of the torsion tube indicate that a torque of 32 N·m is required to achieve a 60° twist. Furthermore, the spring tension F_1 must exert a torque of at least 32 N·m on the output end of the torsion tube. The connection structure at the output end of the torsion tube is connected to a tension spring, and the torque and angle of rotation must be converted in accordance with the following formulae.

$$F_1 = \frac{T}{R} \tag{4}$$

$$\Delta L = \varphi R \tag{5}$$

where F_1 represents the initial tension of the bias spring and ΔL the length of the spring that has been stretched. The circular structure connected to the spring is set up in the connection module with the intention of converting the spring's tension into torque. In accordance with the dimensional relationship of the wingtip structure, the radius of the circular structure is 50 mm, which means that the required F_1 is 1 280 N. As the temperature rises, the SMA torsion tube undergoes a reversible deformation, resulting in further stretching of the spring. It is essential to ensure that the spring does not exceed its elastic range during the stretching process. Once the temperature has been reduced, the torque pro-

vided by the spring consistently exceeds 32 N·m, which can be employed as a substitute for the external loads that directly deform the SMA torsion tube initially.

According to Ref.[15], with three springs in parallel, the parameters of the bias spring mechanism are obtained and can be calculated as follows

$$k = \frac{Gd^4}{8nD_0^3} \tag{6}$$

$$n = \frac{Gd^4 \Delta L_{\text{max}}}{8d^3 (F_n - F_0)} \tag{7}$$

where k is the spring stiffness; G the shear modulus of the spring material; d the diameter of the spring wire; D_0 the mid-diameter of the spring, indicating the average diameter of the spring coil; n the number of active coils in the spring; $\Delta L_{\rm max}$ the maximum working stroke of the spring; F_n the maximum tensile force of the spring; and F_0 the tensile force at its initial state.

Table 2 shows the spring parameters in the current study.

Table 2 Bias spring parameters

Symbol	Value
n	34
d/mm	4
$D_{\scriptscriptstyle 0}/{ m mm}$	25
G/GPa	79
$k/(\mathrm{N} \bullet \mathrm{mm}^{-1})$	4.765
$K/(\mathrm{N}^{ullet}\mathrm{mm}^{-1})$	14.295
$F_{\scriptscriptstyle 1}/{ m N}$	420
F_n/N	500
$\Delta L_{ ext{max}}/ ext{mm}$	21

2. 2 Actuation capacity analysis

The driving process of the actuation mechanism is divided into two parts, namely low temperature and high temperature. The simplified actuation mechanism is a combined mechanism comprising a torsion tube and a tension spring. In the low-temperature state, the torsion tube is subjected to initial torsion by the bias mechanism. In order to find the load characteristics of the torsion tube, the torqueangle relationship derived from the martensite state test is employed. The equivalent torque of the spring and the reaction torque of the SMA torsion

tube can both be expressed as a function of the angle of torsion.

$$F_2 = F_1 + K \cdot \Delta l \tag{8}$$

$$T_1(\varphi) = F_2 \cdot R - \frac{KR^2}{8} \cdot \varphi \tag{9}$$

$$T_{A}(\varphi) = T_{M} - \frac{G_{A}I_{P}}{L} \cdot \varphi \tag{10}$$

where F_1 represents the initial load of the bias mechanism, F_2 the load after the bias mechanism has been stretched, T_1 the variation in equivalent torque of the bias mechanism with respect to the rotation angle in the low-temperature state, T_A the variation in torque with the rotation angle of the SMA torque tube during the heating recovery phase, T_M the torque required for the change of detwinned martensite, G_A the shear modulus of austenite, φ the torsion angle of the SMA torsion tube, R the radius of the connection between the bias mechanism and the torsion tube, I_P the polar moment of inertia of the SMA torsion tube, and Δl the elongation of the bias spring.

Indeed, when the torsion tube is twisted in the martensitic state, the shear modulus of the material is observed to decrease as the material undergoes a stress-induced non-twinned martensitic transformation from the twinned martensitic state. Accordingly, the calculated biasing force, derived from the aforementioned biasing mechanism and based on the initial shear modulus of the martensite in the material, is sufficient to induce the initial deformation of the SMA torsion tube. This is ensured by the pre-assembled limiting mechanism, which maintains the torsion tube within the specified angular range. This is achieved through the use of a pre-installed limiting mechanism, which guarantees that the torsion tube is twisted within a specified angular range. This prevents any additional deformation from occurring, even in the event of a load exceeding the required torque to twist the tube to 60°.

The internal stress state of SMAs during the heating process is complex, and one of the characteristics is that the restoring force increases in proportion to the external load. In order to facilitate the characterization of the torque output capacity of the

torsion tube, its restoring capacity is characterized in accordance with the shear modulus obtained from the testing of its austenitic state. The resulting load curve is presented in Fig.8. The yellow line illustrates the test results for the torque required for torsion of the SMA torsion tube. According to the theoretical torque conversion of the bias mechanism, the blue line represents the equivalent torque provided by the bias mechanism at low temperatures. At high temperature, the red line is also sufficient to drive the external loads and allow the bias mechanism to store part of the energy.

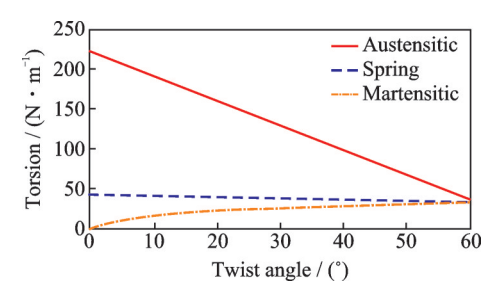


Fig.8 Torsional characteristic curves of drive mechanism

The load provided by the bias mechanism in the low-temperature state is sufficient to induce the specified phase transformation process. Also, the deformation resulting from the austenite transformation is also capable of ensuring a certain load output. Once the bias tension spring is pre-stretched, the actuator can be used in both the forward and backward way.

3 Simulation Analysis and Testing

During the stable level flight phase of the aircraft, the loads on the folding wingtip structure are primarily comprised of the weight of the wingtip structure and the aerodynamic loads. The aerodynamic loads on the wingtip structure are estimated according to the following working conditions. The Tornado VLM, which is an open-source aerodynamic software based on the vortex lattice method (VLM), is applied for the aerodynamic analysis since the flight speed is not very high in the current study, and high-fidelity tools will be used in the detailed analysis. The aerodynamic loads on the wingtip at each folding angle are calculated with the flight conditions outlined in Table 3.

Table 3 Flight condition parameter

Parameter	Value	
Airfoil	NACA2412	
Chord/mm	40	
Angle of attack/(°)	3	
Folding angle/(°)	0-90	
Flight speed/(m•s ⁻¹)	60	
Mass (in physics)/kg	4.192	
Density/ $(kg \cdot m^{-3})$	1.160	

The bending moment distribution on the wing is analysis, which is then used to find the required torque for the folding wingtip, as shown in Fig.9. The required torque is between 4.62 N·m and 10.03 N·m. And it is the largest when the folding angle is 0, and decreases with the increase of the folding angle. The estimation process provides a reference for the design of the folding wingtip mechanism.

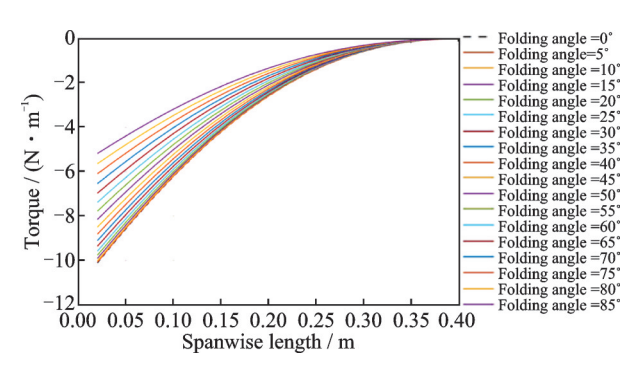


Fig.9 Required folding torque of the wingtip

3. 1 Analysis of wingtip kinematics

The combination of the SMA torsion tube and the bias mechanism allows the actuator to achieve a recoverable turning angle of 60°. Due to the limited space at the wingtip and the required folding angle of 90°, the drive mechanism is designed with a transmission ratio of 1:1.5.

Numerical simulation is performed to find the kinematics of the folding wingtip mechanism, which is performed with the multi-body dynamics software ADAMS®. And Fig.10 shows the model used for the simulation.

The wingtip structure is made of resin and the remaining connecting structure is made of aluminum alloy. Each part must then be assembled according to the system structure. The support structure is affixed to the ground through the constraints and joints in ADAMS. The input and output are configured with joint connections, and the contact properties of the two gear contact surfaces are defined. The dead weight is considered to simulate the loads imposed on the system under actual working conditions. Actuation is then applied to the moving part of the system to find the relationship between the input angle and the output folding angle, as shown in Fig.11.

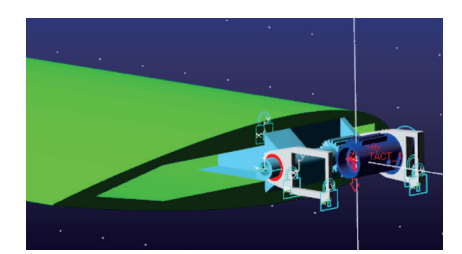


Fig.10 ADAMS model of folding wingtip mechanism

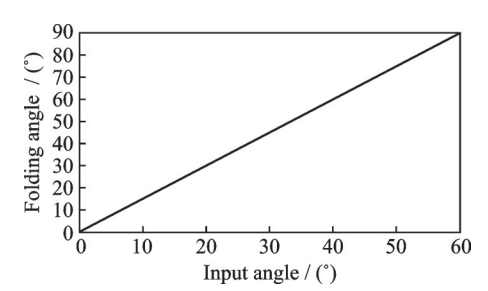


Fig.11 Input angle versus wingtip folding angle

When the wingtip folds upwards, the aerodynamic load on the wingtip is opposed to the direction of gravity, leading to the reduction of the overall loads. Therefore, the motion characteristics are analyzed only considering the inertial load of the wing tip.

In the simulation, a specific torsion angle input is also employed as expressed in the following equation to ensure that the folding process is carried out in a smooth way.

$$\varphi(t) = \frac{\varphi_{\text{max}}}{2} \left(1 - \cos\left(\frac{\pi t}{t_0}\right) \right) \tag{11}$$

where t is the simulation time and t_0 the total time of a single folding.

Fig.12 shows the curve of the input torsion angle. Together with the folding angle curve, the output torque of the folding mechanism can also be found in Fig.13.

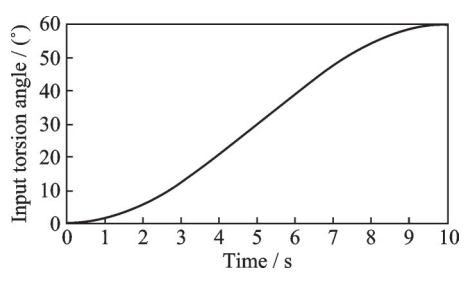


Fig.12 Input torsion angle

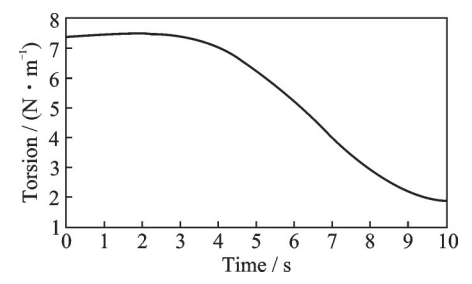


Fig.13 Output torque of folding mechanism

Fig.14 also shows the folding wingtip at different simulation time.

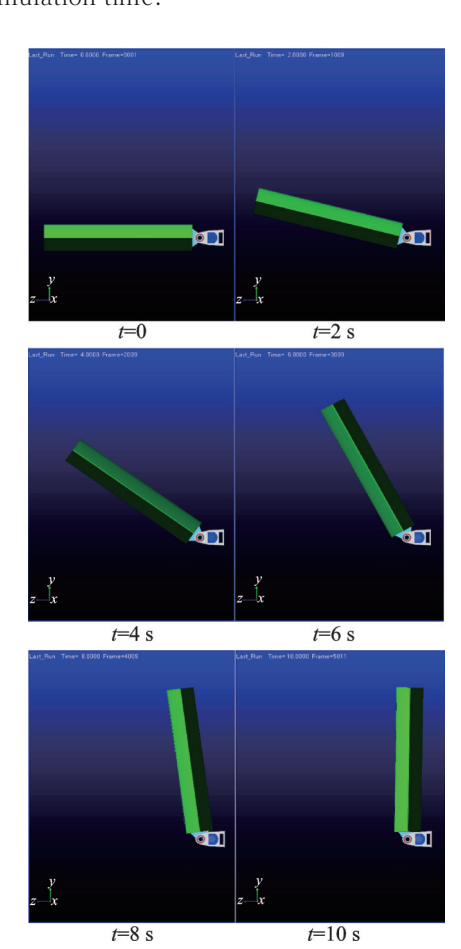


Fig.14 Wingtip folding angle

3. 2 Finite element analysis of the folding structure

In order to verify the folding wingtip structure

during actuation, a finite element model of the folding mechanism is constructed using the commercial software ABAQUS®.

Fig.15 shows the components in the folding mechanism. The supports are fixed as the boundary conditions, and the torsion tube is connected to the supports using the hinge connection in the model, which allows the torsion of the tube. Table 4 summarizes the mesh properties in the folding mechanism.

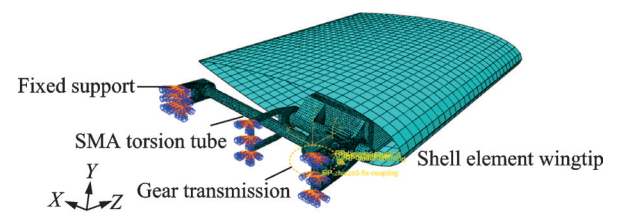


Fig.15 Finite element model of folding wingtip mechanism

Table 4 Mesh properties

Part name	Number of	Number	Maril ton	Element
	element	of node	Mesh type	type
Fixed support 1	3 210	4 499	Hexahedral mesh	C3D8R
Fixed support 2	1 047	1 820	Hexahedral C3D8R	
Fixed support 3	4 806	8 835	Tetrahedral mesh	C3D10
Connection structure	37 376	50 405	Hexahedral mesh Tetrahedral mesh	C3D8RC3 D10
Wingtip beam	26 589	42 005	Hexahedral mesh Tetrahedral mesh	C3D8RC3 D10
Wingtip	1 728	1 792	Quad mesh	S4R

The primary wing structure is made of aluminum. The torsion tube is made of the SMA material. The other part of the wingtip structure is made of resin material. The material parameters are summarized in Table 5.

Table 5 Mesh properties

Performance	Density/	Young's	Poisson's	Strength/
parameter	$(g \cdot cm^{-3})$	modulus/MPa	ratio	MPa
SMA	6.50	32 000	0.3	
Aluminum	2.70	69 000	0.3	230
Resin	1.16	2 300	0.4	25

The simulation will be performed to verify whether the supporting structure can meet the strength requirements. In the low-temperature martensitic state, the SMA torsion tube is in a passively deformed state. The torque from the spring is used for the simulation. In this cases, the SMA torsion

tube in the martensitic state will carry a torque of 32 N·m when the tube has a 60° torsion according to the bias spring mechanism. The torque is applied to the circular structure connected to the spring, and the von Mise stress and displacement distribution is shown in Fig.16.

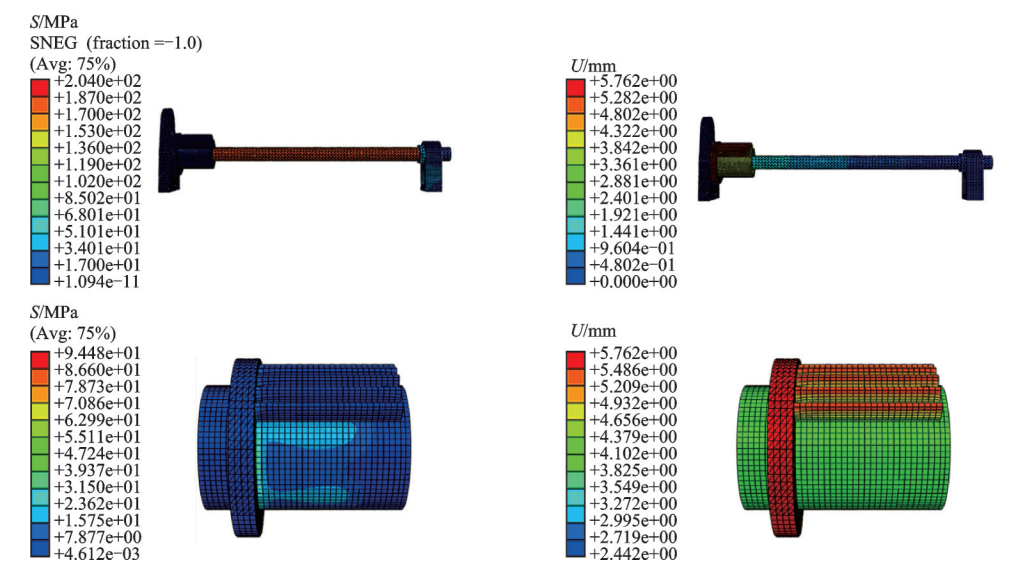


Fig.16 Stress (Left) and displacement (Right) of the tube and support

The simulation results demonstrate that the torsion tube has the greatest stress during passive torsion. In the current study, it is assumed the shear modulus of the SMA torsion does not change in shear modulus due to the transformation from twinned martensite to de-twinned martensite. The connecting structure in the torsion process will transmit the torque to the wingtip structure. The maximum stress is shown to be approximately 95 MPa, which is less than the failure stress of the material.

In the actuation process, the model is simplified by fixing the internal structure of the connecting structure and applying an equivalent torque of 40 N·m. The resulting stress and displacement are presented in Fig.17. The maximum stresse and displacement are observed at the connecting structure again.

The maximum stress is 55.2 MPa and the deformation is 0.01 mm, indicating that the connection structure can carry the loads during the condition, which verifies the folding mechanism conceptually.

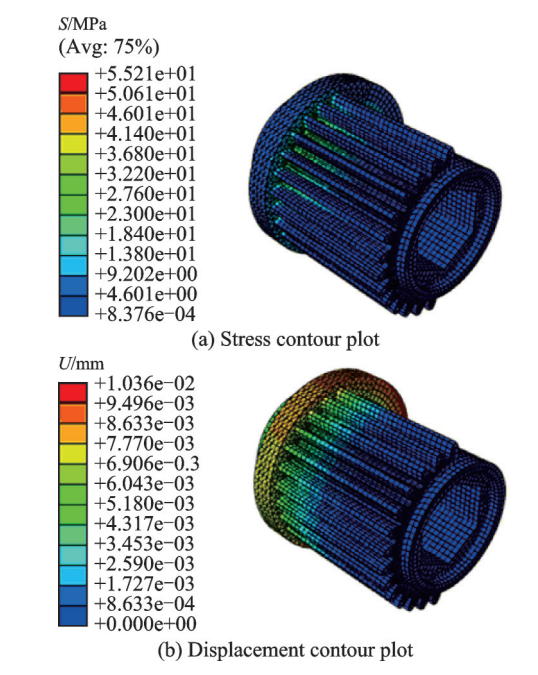


Fig.17 Stress and displacement of the connecting structure

3. 3 SMA torque tube response test

To further verify the concept of the SMA torsion tube, a heating recovery test is conducted under no-load conditions. Considering the structural characteristics of the SMA torsion tube, the built-in

heating and temperature control system is established, as illustrated in Fig.18, which includes a power supply, a programmable logic controller (PLC), a thermocouple, a relay, and a heater.

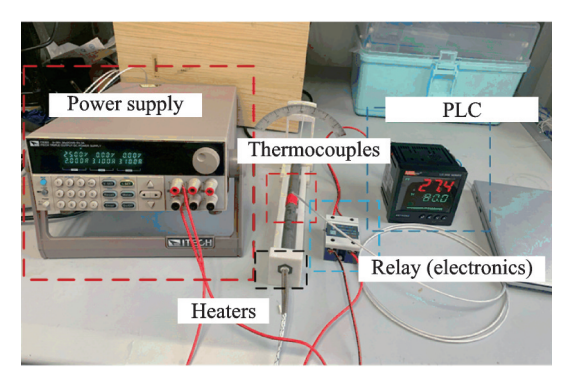


Fig.18 SMA torsion tube temperature control device

The target temperature is controlled by the PLC controller, which sends a control signal to the relay. The relay then controls the heater, which heats the SMA torsion tube. The temperature of the torsion tube is tested as a feedback signal, which is given back to the controller. The controller then controls the heater on and off in order to maintain the temperature.

As the temperature increases, the pre-installed angle pointer can be found to rotate, indicating the change of the torsion angle, which is due to the austenite transformation of the SMA tube. The material undergoes a phase change concurrently with the aforementioned deformation. As the temperature of the entire torsion tube is over the austenitic transformation finish temperature, the material could be regarded as fully transformed, although some residual strain could remain. In the current study, the test SMA torsion tube can undergo a torsion tube of over 30°, as shown in Fig.19.

The response time of the torsion tube is determined by its heating device and the environment temperature. In the current test, since the focus is to verify the concept, a relatively low heating power is applied, with the heating rod operated at 24 V and 3 A. The tube torsion angle is recovered from 42° to 5° in around 160 s. Obviously, the time period can be reduced significantly in the real-world application

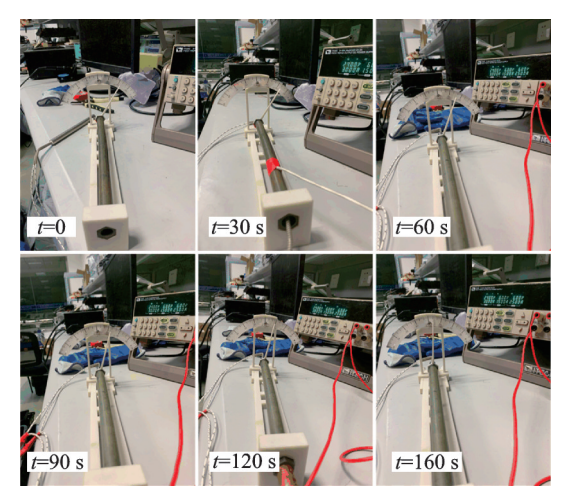


Fig.19 SMA torsion tube heating response test

with an increased heating power.

4 Conclusions

A folding wingtip structure based on the SMA torsion tube is proposed. After analyzing the characteristics of SMA torsion tubes, the required actuation conditions are determined, and SMA torsion tubes with shape memory effect are prepared. Tests are conducted to identify the phase transition temperature and the stress-strain behavior in different states. A bias spring mechanism is designed, showing that the wingtip folding from 0° to 90° is available.

Numerical simulation is carried out to verify the structural design by finding the kinematics relationship of the mechanism and the stress and strain distribution. Furthermore, a heating recovery test is conducted, which demonstrates the feasibility of the SMA torsion tube as an actuator of the folding wingtip.

In future research, a more comprehensive and in-depth exploration of the SMA torsion tube will be conducted. The temperature control system will be integrated in the future work for the real-world application of the SMA tube. Additionally, a thermo-mechanical coupling model will also be developed to rapidly predict the mechanical properties and the required temperature of the SMA torsion tube, which can lay a solid foundation for the future applications.

References

- [1] LI D, ZHAO S, DA RONCH A, et al. A review of modelling and analysis of morphing wings[J]. Progress in Aerospace Sciences, 2018, 100; 46-62.
- [2] DUSSART G X, MUDASSIR L, et al. In-flight wingtip folding: Inspiration from the XB-70 Valkyrie[J]. International Journal of Aviation, Aeronautics, and Aerospace, 2019, 6(3): 7.
- [3] WAN L, WANG C, MAO Y, et al. Experimental study and analysis of gust load alleviation using folding wingtips[C]//Proceedings of the 18th National Conference on Aeroelasticity. 2023: 487-494.
- [4] MILLS J, AJAJ R. Flight dynamics and control using folding wingtips: An experimental study[J]. Aerospace, 2017, 4(2): 19.
- [5] PAN G, CUI X, SUN P, et al. A brief review of the actuation systems of the morphing systems in wind tunnel models and a case study[J]. Aerospace, 2024, 11 (8): 666.
- [6] HE Z, FAN S, WANG C, et al. Conceptual design of compliant structures for morphing wingtips using single-row corrugated panels[J]. Aerospace, 2024, 11 (8): 682.
- [7] JANI J M, LEARY M, SUBIC A, et al. A review of shape memory alloy research, applications and opportunities [J]. Materials & Design, 2014, 56: 1078-1113.
- [8] SUN J, GUAN Q, LIU Y, et al. Morphing aircraft based on smart materials and structures: A state-of-the-art review[J]. Journal of Intelligent material systems and structures, 2016, 27(17): 2289-2312.
- [9] LIW, XIONG K, CHEN H, et al. Research on variable cant angle winglets with shape memory alloy spring actuators[J]. Acta Aeronautica et Astronautica Sinica, 2012, 33(1): 22-33.
- [10] JAYANTH N, SANDERS B P, PINKERTON-FLORANCE, et al. Overview of the DARPA/AFRL/NASA smart wing phase II program[C]//Proceedings of Industrial and Commercial Applications of Smart Structures Technologies. Bellingham: SPIE, 2001, 4332: 383-389.
- [11] BENAFAN O, MOHOLT M R, BASS M, et al. Recent advancements in rotary shape memory alloy actuators for aeronautics[J]. Shape Memory and Superelasticity, 2019, 5(4): 415-428.
- [12] STROUD H, HARTL D. Shape memory alloy tor-

- sional actuators: A review of applications, experimental investigations, modeling, and design[J]. Smart Materials and Structures, 2020, 29(11): 113001.
- [13] CALKINS F T, NICHOLSON D E, VONDEET-ZEN S, et al. Low & high speed cryogenic testing of a wind tunnel model with remote control actuation (RCA) spoiler[C]//Proceedings of AIAA Aviation 2019 Forum. [S.l.]: AIAA, 2019; 2975.
- [14] ICARDI U, FERRERO L. Preliminary study of an adaptive wing with shape memory alloy torsion actuators[J]. Materials & Design, 2009, 30(10): 4200-4210.
- [15] CHENG Daxian. Mechanical design manual[M]. 6th ed. Beijing: Chemical Industry Press, 2016. (in Chinese)

Acknowledgements This work was supported by the National Natural Science Foundation of China (No.52305262), the Aeronautical Science Foundation of China (No.20230015052002), and the Fundamental Research Funds for the Central Universities (No.NT2024001).

Authors

The first author Mr. LAI Zhenyang received his M.S. degree in mechanical engineering from Nanjing University of Aeronautics and Astronautics, specializing in morphing aircraft. He has become an engineer at the China Special Vehicle Institute since April 2025.

The corresponding author Prof. WANG Chen received his B.S. and M.S. degrees from Nanjing University of Aeronautics and Astronautics, and his Ph.D. degree in Swansea University. His research interests include morphing aircraft, smart structures and structural dynamics.

Author contributions Mr. LAI Zhenyang conducted the simulation and experimental tests, and wrote the manuscript. Prof. WANG Chen proposed the initial concept, guided the research, refined and edited the manuscript. Mr. YANG Yang contributed to the design and experiment tests. Mr. WAN Liliang contributed to the numerical simulation. Prof. SHEN Xing contributed to the manuscript editing and overall guidance. All authors commented on the manuscript draft and approved the submission.

Competing interests The authors declare no competing interests.

用于变体飞行器折叠翼尖机构的形状记忆合金扭力管设计

赖振洋,王 晨,杨 洋,万里亮,沈 星

(南京航空航天大学航空学院,南京 210016,中国)

摘要:变体飞行器可以根据飞行任务变化改变自身外形,从而在未来应用中具有更好的性能。折叠翼尖具有提升航程、提升机动性、减缓载荷、提高机场通过性等潜在优势,是变体飞行器的重要研究方向之一。本文提出了一种基于形状记忆合金扭力管的折叠翼尖机构设计,利用形状记忆合金的驱动特性实现机翼翼尖的折叠。该设计采用形状记忆合金扭力管作为驱动器,充分利用记忆合金管易于集成、能量密度相对较高的特点。本文通过数值仿真与试验,初步验证了该设计方案,展现了形状记忆合金扭力管在折叠翼尖驱动器上的应用潜力。 关键词:变体飞行器;折叠翼尖;形状记忆合金扭力管